Bioactive Materials 41 (2024) 15–29

Contents lists available at ScienceDirect

Bioactive Materials

journal homepage: www.keaipublishing.com/en/journals/bioactive-materials

Oriented cellulose hydrogel: Directed tissue regeneration for reducing corneal leukoplakia and managing fungal corneal ulcers

Lina Dong [a,b,1], Zixin Fan [c,1], Bixing Fang [d], Xiaoyu Zhao [a], Hongyi Yao [a], Gangpei Cai [a], Shuo Yang [c], Guoming Zhang [c], Xiaoqi Cheng [a], Yun Feng [g,*], Shengli Mi [a,*], Wei Sun [a,e,f,*]

[a] Tsinghua Shenzhen International Graduate School, Tsinghua University, Shenzhen, 518055, China
[b] Department of Burns, The Second Affiliated Hospital, Zhejiang University School of Medicine, Zhejiang, China
[c] Shenzhen Eye Hospital, Jinan University, Shenzhen Eye Institute, Shenzhen, Guangdong, 518040, China
[d] Department of Otolaryngology, The Second Affiliated Hospital, Zhejiang University School of Medicine, Zhejiang, China
[e] Department of Mechanical Engineering, Biomanufacturing Center, Tsinghua University, Beijing, China
[f] Department of Mechanical Engineering, Drexel University, Philadelphia, PA, USA
[g] Department of Ophthalmology, Peking University Third Hospital, Beijing, 100191, China

ARTICLE INFO

Keywords:
Corneal leukoplakia
Fungal corneal ulcers
Oriented tissue regeneration
Nanozyme
Cellulose hydrogel

ABSTRACT

Fungal corneal ulcer is one of the leading causes of corneal blindness in developing countries. Corneal scars such as leukoplakia are formed due to inflammation, oxidative stress and non-directed repair, which seriously affect the patients' subsequent visual and life quality. In this study, drawing inspiration from the oriented structure of collagen fibers within the corneal stroma, we first proposed the directional arrangement of CuTA-CMHT hydrogel system at micro and macro scales based on the 3D printing extrusion method combined with secondary patterning. It played an antifungal role and induced oriented repair in therapy of fungal corneal ulcer. The results showed that it effectively inhibited *Candida albicans, Aspergillus Niger, Fusarium sapropelum*, which mainly affects TNF, NF-kappa B, and HIF-1 signaling pathways, achieving effective antifungal functions. More importantly, the fibroblasts interacted with extracellular matrix (ECM) of corneal stroma through formation of focal adhesions, promoted the proliferation and directional migration of cells *in vitro,* induced the directional alignment of collagen fibers and corneal stromal orthogonally oriented repair *in vivo*. This process is mainly associated with MYLK, MYL9, and ITGA3 molecules. Furthermore, the downregulation the growth factors TGF-β and PDGF-β inhibits myofibroblast development and reduces scar-type ECM production, thereby reducing corneal leukoplakia. It also activates the PI3K-AKT signaling pathway, promoting corneal healing. In conclusion, the oriented CuTA-CMHT hydrogel system mimics the orthogonal arrangement of collagen fibers, inhibits inflammation, eliminates reactive oxygen species, and reduces corneal leukoplakia, which is of great significance in the treatment of fungal corneal ulcer and is expected to write a new chapter in corneal tissue engineering.

1. Introduction

Fungal keratitis is a common cause of corneal ulcers and a leading cause of eye-related morbidity and blindness, particularly in tropical and subtropical regions [1–3]. Fungal keratitis can give rise to severe infections, potentially resulting in blindness and vision loss [4,5].During the evolution of the disease, severe inflammatory reactions [6], oxidative stress [7,8], and non-directional repair processes, easily leading to the formation of corneal scars, such as leukoplakia [9–11]. It will diminishing corneal transparency and significantly impairing both the visual acuity and overall quality of life for affected individuals. Globally prediction over 100,0000 cases annually, there is an urgent need for effective therapeutic of fungal keratitis, especially inhibiting the corneal leukoplakia. Contemporary therapeutic approaches for fungal keratitis include drug treatments and surgical interventions [12–15].Common pharmaceutical options include the Amphotericin B and Fluconazole [16]. However, their usage is limited due to associated toxicity. Surgical treatments primarily involve corneal transplants. Existing challenges in

Peer review under responsibility of KeAi Communications Co., Ltd.
* Corresponding author.
E-mail address: weisun@mail.tsinghua.edu.cn (W. Sun).
[1] Lina Dong and Zixin Fan contributed equally to this work.

https://doi.org/10.1016/j.bioactmat.2024.07.008
Received 2 March 2024; Received in revised form 18 June 2024; Accepted 4 July 2024

current strategies are as follows: (1) Non-directional repair in the corneal stromal layer, leading to the easy formation of leukoplakia. (2) Limited efficacy of antifungal drugs and appearing the severe inflammatory responses during the illness. (3) Oxidative stress damage to cells and worse suboptimal corneal healing.

Recently, both domestic and international research has focused on the development of hydrogel systems for the treatment of fungal keratitis [17–21], utilizing microneedles [22–25], three-dimensional (3D) printing [26,27], and electrospinning methods [28]. However, these hydrogel systems often have individual shortcomings: hydrogel systems typically exhibit a single functionality, provide less intervention in the corneal ulcer healing process, and fail to address the comprehensive aspects of antifungal, anti-inflammatory, directed repair of the corneal stromal layer, and inhibition of leukoplakia formation. More importantly, most studies ignore the unique collagen fiber directional arrangement of the cornea in their design, which could impact the therapeutic efficacy against leukoplakia. Therefore, based on our team's previous research [29–33], we have developed a novel multifunctional hydrogel system to treat fungal keratitis, reduce leukoplakia, and promote healing by integrating antifungal, anti-inflammatory, and directed repair properties. Furthermore, we have delved into the biological mechanisms underlying the inhibition of leukoplakia.

In this study, drawing inspiration from the oriented structure of collagen fibers within the corneal stroma, we propose an oriented CuTA-CMHT hydrogel system (Scheme 1A). The system formed by combining the copper-tannic acid nanozyme (CuTA) and hyaluronic acid-tannic acid (HA-TA) composite with carboxymethyl cellulose-methacrylate (CMC-MA) hydrogel, which had the following advantages: (1) Employing 3D printing extrusion combined with secondary patterning, the hydrogel achieves an orderly directional arrangement at both micro and macro levels (Scheme 1B-E). Protrusion of fibroblasts senses the topological structure of hydrogel and orient themselves along with the micropatterned lines. Besides, the fibroblasts also interacted with ECM of corneal stroma through formation of focal adhesions. This process is associated with molecules such as MYLK, MYL9, and ITGA3. Furthermore, the downregulation the growth factors TGF-β and PDGF-β, inhibits myofibroblast development and reduces scar-type ECM production, thereby reducing corneal leukoplakia. (2) By introducing Cu^{2+} to mediate the oxidative coupling assembly of tannic acid, we designed copper-tannic acid nanozymes. These nanozymes primarily affect signaling pathways such as TNF, NF-kappa B, and HIF-1, resulting in effective antifungal and anti-inflammatory characteristics. The CuTA nanozyme is assembled by introducing Cu^{2+} to mediate the oxidative coupling of TA, which mainly affects signaling pathways such as TNF, NF-kappa B, HIF-1, achieving effective antifungal and anti-inflammatory properties. (3) The CMHT hydrogel reduces oxidative stress damage and activates the PI3K-AKT signaling pathway, promoting corneal healing (Scheme 1F, G).

In summary, our proposed CuTA-CMHT hydrogel system exhibits characteristics such as antifungal, anti-inflammatory properties, reduction of corneal leukoplakia, and promotion of healing. It exhibits great promise in the treatment of fungal corneal ulcers and leukoplakia, potentially achieving groundbreaking progress in corneal tissue engineering.

2. Materials and methods

2.1. Reagents and materials

Hyaluronic acid (HA, MW 100–200 kDa) was purchased from Lifecore Biomedical (Chaska, MN, USA). Methacrylic anhydride (MA) and Irgacure 2959 were purchased from Sigma–Aldrich (St. Louis, MO, USA). The cotton linter pulps were provided by Hubei Chemical Fiber Group Ltd. (Xiangfan, China). Other analytical grade chemicals were purchased from Sinopharm Chemical Reagent Co., Ltd. (Shanghai, China).

2.2. Synthesis of CMHT hydrogels

Prepare the 1 % carboxymethyl cellulose (CMC) solution and stir it at 50 °C for 1 h 5 % cellulose nanofiber (CNF) were further introduced into the mixture [33]. Subsequently, excess methyl acrylate was added to the CMC solution (4 °C, 24 h). The pH was adjusted to 8, followed by purification through a 96-h dialysis process. The purified carboxymethyl cellulose methacrylate (CMCMA) was obtained after freeze-drying and stored at −20 °C. In addition, the HATA were fabricated through a physical crosslinking mechanism involving the formation of hydrogen bonds between the hydroxyl (-OH) groups present in hyaluronic acid (HA) and tannic acid (TA). Dissolve HA in a 0.2 M MES buffer solution to obtain a 2 wt% HA solution (pH 5.5). Subsequently, the HA solution was combined with a TA solution in a ratio of 1:4. Subsequently, 10 % CMCMA was introduced with concentration ratios of CMCMA:HATA at 2:1, 1:1, and 1:2, yielding various compositions of CMHT hydrogels.

2.3. Synthesis of CuTA nanozyme

Dissolve 27 mg of tannic acid and 875 mg of $CuSO_4{\cdot}5H_2O$ in 50 mL of deionized water. Following PH adjustment to 7.4 with 1 M NaOH, the solution was heated to 50 °C. The resulting product was separated via centrifugation and thoroughly washed 5 times with DI water. CuTA nanozyme was obtained after freeze-drying.

2.4. Synthesis of CuTA-CMHT hydrogel

The addition of CuTA nanozyme at different masses were evenly dispersed into the CMHT solution, yielding the CuTA-CMHT hydrogel (12.5 μg/mL, 25 μg/mL, 50 μg/mL, 100 μg/mL, 200 μg/mL).

2.5. Rheological tests of hydrogels

Rheological assessments were conducted using a rheometer (MCR302, Anton Paar, Austria) equipped with a plate-plate geometry (25 mm in diameter and a 27 μm gap). Shear viscosity measurements were carried out over shear rates ranging from 1 to 100 s^{-1} at 25 °C. Oscillatory frequency sweep was performed at 0.5 % strain and frequencies of 0.1–10 Hz. All tests were conducted within the linear viscoelastic region, and the experiments were repeated three times for the various ratio of the hydrogels.

2.6. 3D printing of the CuTA-CMHT hydrogel

High-precision digital light processing (DLP) manufacturing (Polytech) was employed to 3D print commercial resin × 22, creating a precise microstructure for mold preparation. Subsequently, a flexible mold was produced through polydimethylsiloxane (PDMS) infusion, and surface plasma treatment was applied to reduce bonding strength. This method yielded a groove model with length and width are 1 cm, with groove spacing of 100 μm, a width of 100 μm, and a depth of 150 μm.

The hydrogel precursors were loaded into a 5 mL syringe. Biomaker software facilitated the design of the printing model, and a 3D printer (SunP CPD1/Biomaker) was utilized to print the CuTA-CMHT hydrogel. A 25 G needle was utilized throughout the process. Printing occurred at 4 °C, with a speed of 10 mm/s and an extrusion rate of 3 mm^3/s. The CuTA-CMHT hydrogel experienced shear thinning within the extrusion needle and then restored its viscosity upon exiting the needle. Consequently, the hydrogel could be printed the uniform 1D filaments and 3D structures on the PDMS mold (Scheme 1E). Post-printing, the structures were exposed to UV light to enhance their stability and gentle peeling from the mold.

2.7. In vitro antifungal test of CuTA-CMHT

In vitro antifungal activity of the CuTA-CMHT was assessed by

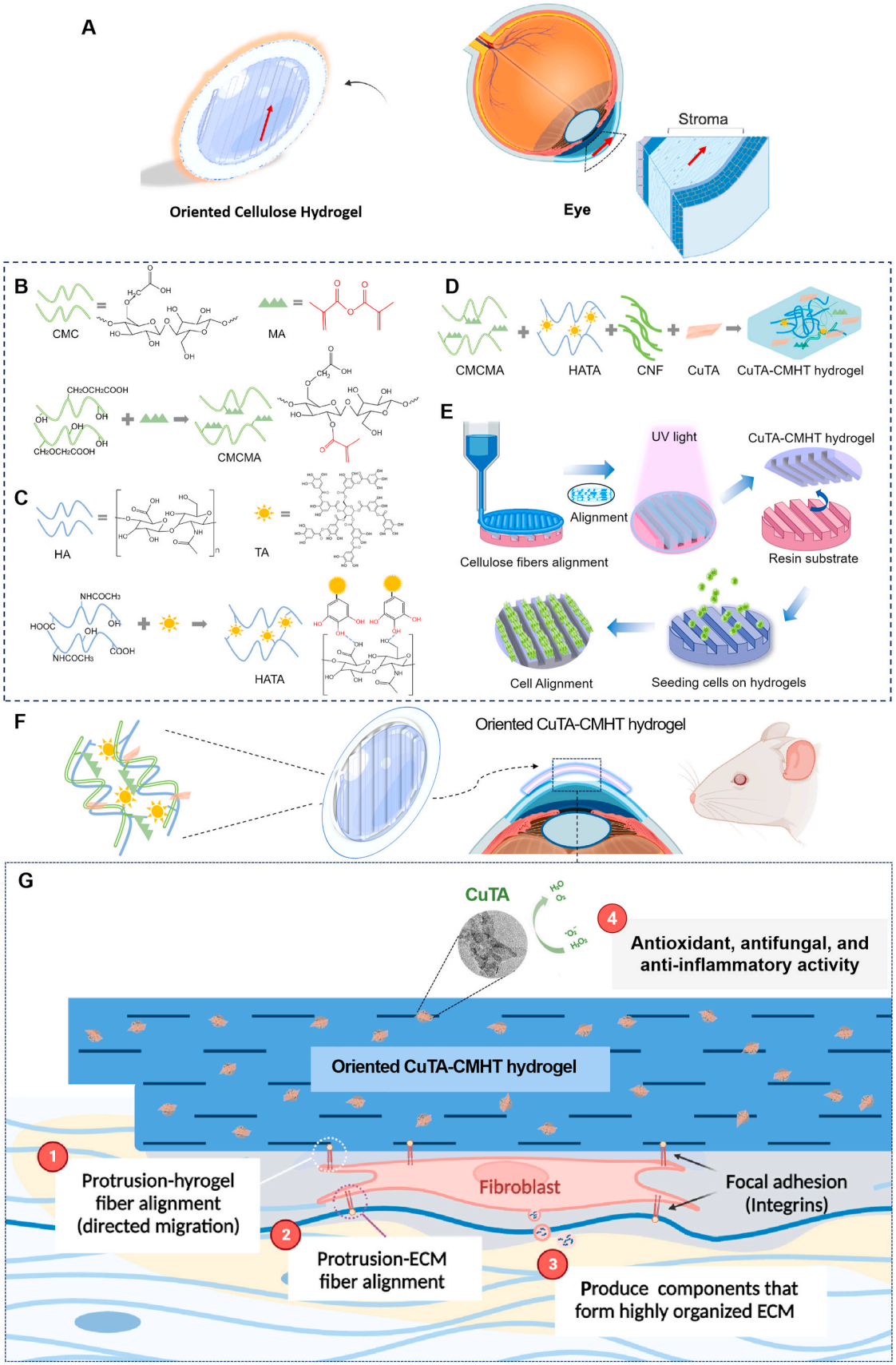

Scheme 1. (A) Schematic illustration of directional-structured CuTA-CMHT hydrogel. (B–E) Schematic of the composition and synthesis mechanism of the oriented-CuTA-CMHT hydrogel. (F, G) Schematic diagram illustrating the mechanism of hydrogel employed for directed repair of corneal stroma and its anti-oxidative, antifungal, and anti-infective properties.

computing the antifungal rate. The *Candida albicans*, *Fusarium solani, Aspergillus niger* were co-cultured with varying concentrations of CuTA-CMHT for 48 h on a shaker (28 °C, 150 rpm). Following the 48-h co-cultivation period, 10 μL of the solution was diluted 10^5 times with PBS and evenly spread on Potato Dextrose Agar. Observe and take photographs after the cultivation period (3–7 days). To assess the *in vitro* antifungal efficacy of CMHT-CuTA, precursor solutions of CuTA-CMHT hydrogel with varied concentrations were formulated, and equivalent concentrations of fungi were introduced. Fluconazole was employed as a positive control. The material was then incubated with the fungal specimens in a well plate for 48 h at 28 °C. Subsequently, MTT reagent was added after the aforementioned experimental procedures and allowed to incubate for 4 h. The optical density at 490 nm (OD_{490}) was measured using a microplate reader.

2.8. SEM images of fungi in antifungal experiments

Different concentrations of CuTA-CMHT (12.5 μg/mL, 25 μg/mL, 50 μg/mL, 100 μg/mL, 200 μg/mL) were co-cultured separately with 1 × 10^5 CFU/mL *Candida albicans*, *Fusarium solani, Aspergillus niger* for 6 h. The pellet was washed 3 times with PBS after centrifugation (3000 rpm) and suspended in a 2.5 % glutaraldehyde solution for 3 h. Following centrifugation, the pellet was washed with PBS. The precipitate was dehydrated in ethanol solutions (20 %, 45 %, 75 %, 90 %). Subsequently, dehydration was continued in 100 % ethanol for 15 min, followed by centrifugation to remove the supernatant. The sample was then placed in a mixture of ethanol and tert-butanol (1:1) and remove the supernatant. Further using pure tert-butanol to wash twice. Finally, 10 μL of the sample was pipetted onto a silicon wafer. Freeze-dry the samples overnight and analyzed by SEM.

2.9. Cellular ROS assessment

Employing corneal epithelial cells to conduct an intracellular ROS scavenging assay. Seed corneal epithelial cells in a 24-well plate, ensuring an equal distribution of cells in each well. Introduce the CuTA-CMHT (12.5 μg/mL, 25 μg/mL, 50 μg/mL, 100 μg/mL, 200 μg/mL) into the experimental group and incubate them for 6 h. Subsequently, wash the cells three times with warm HBSS. As a negative control, treat with 0.1 mM H_2O_2 at 37 °C for 2 h. Then prepare the probe incubation solution DCFH (10 μM). Remove the culture medium, add 500 μL of the probe working solution to each well, and incubate in a 37 °C incubator for 20 min. Afterward, remove the probe incubation working solution, and add 400 μL of culture medium to each well. Observe intracellular green fluorescence using confocal microscopy. For the quantitative detection of cellular ROS levels, repeating the above steps. Seeding the corneal epithelial cells in a 96-well plate. Add 100 μL of probe solution DCFH to each well and incubate in a 37 °C incubator for 20 min. Wash with HBBS, add 100 μL culture medium to each well, and detect fluorescence intensity on a Fluorescent Microplate Reader.

2.10. Cell seeding and cell cultures on scaffolds

The secondary patterned CuTA-CMHT hydrogel scaffold was immersed in culture medium and soaked overnight at 4 °C. Corneal stromal cells were cultured in DMEM F12 medium supplemented with 10 % fetal bovine serum (FBS) at 37 °C and 5 % CO_2. A corneal stromal cell suspension with a density of 5 × 10^6 cells/mL was seeded onto the scaffold. The scaffolds were cultured at 37 °C with 5 % CO_2, and the medium was changed every two days. All data were expressed as at least three independent experiments.

2.11. Cytotoxicity test of different ratio of CuTA-CMHT hydrogels

Corneal epithelial cells at a density of 4 × 10^4 cells/mL were seeded into a 48-well plate and incubated for 24 h. Then, the cells were co-cultured with crosslinked CuTA-CMHT hydrogels scaffold sheets. Following co-culture for 1, 3, and 7 days, CCK8 solution was added and incubated for 2 h. The reaction solution was then transferred to a 96-well plate, and the OD at 450 nm was measured using a spectrophotometer.

2.12. Live/dead staining of corneal epithelial cells

Following the same procedure as above, epithelial cells were co-cultured with CuTA-CMHT hydrogels for 7 days. To stain live and dead cells, Calcein-AM/ethidium homodimer dye was added for 15 min. The results were observed using a Leica DMi8 fluorescence microscope.

2.13. Cell migration assessment

Epithelial cells at a density of 5 × 10^5 cells/well were cultured in 6-well plates for 24 h. Scratches of the same width were made at the bottom of the wells, followed by three washes with PBS. Epithelial cells were then co-cultured with immersion solution of CMHT hydrogel and CuTA-CMHT hydrogel for 24 h. The migration rate of the cells in the scratch area was observed under a microscope and photographed for quantitative analysis.

2.14. In vitro anti-inflammatory effect of CuTA-CMHT hydrogel

Lipopolysaccharides (LPS)-triggered macrophages model [34] and *Candida albicans*-triggered human corneal epithelial cells model [35] were used to investigate the anti-inflammatroy effect of CuTA-CMHT hydrogel *in vitro*. RAW264.7 cells cultured in 6-well plates (1 × 10^4 cells mL^{-1}) were incubated for 24 h. The cells were preconditioned with 50 ng/mL LPS for 12 h, washed by PBS for three times, and subsequently treated with CuTA-CMHT(100 μg/mL). Pro-inflammatory mediators expression in the control group, LPS group, and LPS + CuTA-CMHT group was compared by using real-time quantitative polymerase chain reaction (RT-qPCR).

The corneal epithelial cells were cultured in 6-well plates (1 × 10^6 cells/well). After incubated for 48 h, the cells were stimulated with inactivated *Candida albicans* hyphae (5 × 10^6 CFU/mL) for 1 h and treated with CuTA-CMHT or PBS. After 4 h of *Candida albicans* stimulation, cells were collected for to dected mRNA levels of pro-inflammatory mediators in the control group, *Candida albicans* group, and *Candida albicans* + CuTA-CMHT group.

2.15. In vivo therapeutic efficacy and safety experiments

Therapeutic efficacy was evaluated in Sprague Dawley male rats aged 6–8weeks from Guangdong Medical Laboratory Animal Center. Rats were raised in specific pathogen-free environment. All the protocols for animal experiments were approved by the Institutional Animal Care and Use Committee of Tsinghua University and conducted in accordance with the Association for Research in Vision and Ophthalmology statement for the use of animals in ophthalmic vision and research. The rats were individually housed under constant temperature (22 ± 1 °C) and humidity on a 12 h light-12 h dark cycle with free access to food and water. Under anesthetization, models of fungal corneal ulcer were established in the right eyes of the rats via injection in corneal stroma with 1 × 10^6 CFU/mL *Candida albicans*. Fourty-8 h after *Candida albicans* incubation, modeled rats were randomly divided into 5 groups (n = 10) and treated with phosphate buffer saline (served as control), CMHT, fluconazole, CuTA-CMHT, and oriented CuTA-CMHT, respectively. The oriented CuTA-CMHT hydrogel was different from the CuTA-CMHT hydrogel for it had oriented topology. The 5 different interventions were implemented by topically administering drops (25 μL) or hydrogels (equivalent to 25 μL) into conjunctival sac under anesthetization per day for the following 7 days. Corneas were observed and anterior segment photography was performed for 7 consecutive days, with disease

severity assessed by clinical total score (range 0–12) with 3 components (each range 0–4), including area of corneal opacity, density of corneal opacity, and surface regularity (Table S1) [35]. Ulcer area was analyzed using Image J software (National Institutes of Health, Bethesda, MD, USA). Eyes were harvested on days 1, 3, 5, and 7, followed by histopathologic examination with H&E and Masson's trichrome staining. Transcriptome analysis and immunofluorescence were performed on day 3 and day 5, respectively. Furthermore, heart, liver, spleen, lung, and kidney tissues of healthy rats and rats treated with fluconazole and oriented CuTA-CMHT were taken on day 7 and stained with H&E to evaluate the safety of the proposed therapy. The scheme was shown as Fig. 4A.

2.16. H&E and Masson's trichrome staining

According to the standard protocol, tissues were fixed with 10 % formalin, dehydrated, and waxed. Embedded in paraffin, eye specimens were cut into 5-μm-thick cross-sections across cornea center and stained with Haematoxylin-Eosin Staining kit and Masson's Trichrome Staining Kit. As for heart, liver, spleen, lung, and kidney specimens, only H&E staining was performed. Images were captured with a Pannoramic MIDI scanner (3DHISTECH Ltd., Budapest, Hungary).

2.17. Transcriptome analysis

In brief, according to the standard protocol, total RNA of the corneal samples in the 5 groups on day 3 together with healthy corneas were extracted and sequenced using NovaSeq6000 (Illumina Inc., San Diego, CA, USA). Data were analyzed with R software (The R Foundation, Indianapolis, IN, USA). DEGs was identified based on fold change$\geq$ 1.5 and $P < 0.01$ between different groups. Venn diagram, volcano plot, and heatmap were depicted to visualize the upregulated and downregulated DEGs. GO and KEGG enrichment analysis and PPI analysis were implemented and visualized.

2.18. Immunofluorescence staining

According to the manufacturer's protocols, after blocking, the cross-sections of eye specimens on day 5 were incubated overnight at 4 °C with the primer antibodies, including rabbit antibodies specific to MYLK, MYL9, ITGA3, α-SMA, TGF-β, and PDGF-β (Bioss Inc., Woburn, MA, USA) for immunofluorescence staining. After washes, cross-sections were further incubated with anti-rabbit IgG secondary antibodies (Thermo Fisher Scientific, Waltham, MA, USA) for 1 h at room temperature. Nuclei were stained with 4′,6-diamidino-2-phenylindole (DAPI; Sigma-Aldrich Corp., St. Louis, MO, USA). Images were captured with a Pannoramic MIDI scanner (3DHISTECH Ltd., Budapest, Hungary).

2.19. RT-qPCR

To analyze mRNA expression of representative pro-inflammatory mediators (interleukin (IL)-1β and IL-6), total cellular or corneal RNA was extracted using TRIzol reagent, with reverse transcription carried out using the RevertAid First Strand cDNA Synthesis Kit (Thermo Fisher Scientific, Waltham, MA, USA). RT-qPCR was subsequently performed. The $2-\Delta\Delta Ct$ method was used to normalize the relative mRNA expression of the candidate genes to the mRNA expression of GAPDH in each sample.

2.20. Statistical analysis

All data were expressed as at least three independent experiments. The data in Fig. S9 were analyzed with Kruskal-Wallis test & inter-group pairwise comparison, Fig. S19 was analyzed with Student's *t*-test, and transcriptome analysis were analyzed with R, all the data else were analyzed using one-way ANOVA. Significant differences are indicated at $^{*}P < 0.05$, $^{**}P < 0.01$,and $^{***}P < 0.001$.

3. Results and discussion

3.1. Preparation and characterization of CuTA-CMHT hydrogel

We functionalized carboxymethylcellulose with MA groups through hydroxyl esterification, as confirmed by 1H NMR (Fig. 1E and F). This modification enabled UV-responsive in-situ gelation. Additionally, cellulose nanofibers (CNF) were incorporated to enhance mechanical stability and facilitate directional alignment during 3D printing extrusion. Recognizing the inherent weakness in the hydrogel stability of a single network, we introduced the HATA hydrogel network, formed through hydrogen bonding. Tannic acid (TA) in the network possesses antioxidant properties and a catechin structure, enhancing adhesion as a structural stabilizer. TA also functions as an effective cross-linking agent, thereby increases the mechanical properties of the hydrogels. In order to achieve the desired porosity and explore the optimal 3D printing concentration, we prepared composite hydrogels of CMCMA: HATA at 1:2, 2:1, and 1:1 by adjusting the ratios of two hydrogels networks. SEM images of cross-sections and surfaces of the CMHT hydrogel at different proportions are presented in Fig. 1A–D. The CMHT hydrogel with these three ratios exhibits varying pore sizes and porosities, with ratios of 1:1 and 1:2 showing porosities exceeding 60 %, and the pore sizes ranging from 50 to 200 μm (Fig. 1G and H). This pore size range is conducive to cell nutrient exchange as hydrogel scaffold.

To confer antioxidant and antifungal properties upon the CMHT hydrogel, copper-based nanozymes were introduced. Notably, the tannic acid (TA) component exhibits a dual identity. It adeptly establishes a hydrogen bonding network with hyaluronic acid (HA) within the CMHT hydrogel, while concurrently exhibits robust chelating capabilities. TA also engages in oxidative coupling assembly, contributing to the synthesis of CuTA nanozyme. The morphology of the CuTA nanozyme was observed to be flake-like in scanning electron microscopy (SEM), transmission electron microscopy images and element distribution of Cu element (Fig. 1I - L). Fourier transform infrared spectroscopy (FTIR) and X-ray photoelectron spectroscopy (XPS) were utilized for structural characterization, confirming the presence of TA in the CuTA nanozyme. Oxidation and coordination of tannins with Cu^{2+} led to peak splitting and shifting in the FTIR spectrum, particularly concentrating at 3380 cm^{-1}. This phenomenon suggests the disruption of HO–C vibrations after TA coordination with Cu^{2+} (Fig. 1M). The coordination with Cu^{2+} additionally enhanced the thermal stability of the nanozyme (Fig. 1N).

In addition, X-ray diffraction (XRD) patterns revealed distinct diffraction peaks, indicating a specific crystal structure of the CuTA nanozyme (Fig. 1O). The XPS spectrum and elemental analysis spectrum of the CuTA nanozyme confirmed the primary constituents of the nanozyme are C, O, and Cu elements (Fig. 1P and S1). As depicted in Fig. 1Q, the high-resolution spectrum of Cu 2p exhibits prominent peaks at 933.8 eV and 953.5 eV, corresponding to Cu 2p3/2 and Cu 2p1/2, respectively. Deconvolution of the X-ray Auger spectra of Cu LMM reveals two distinct peaks associated with Cu^{2+} and Cu. The analysis indicates that over 90 % of Cu remains in the Cu^{2+} state (Fig. 1R). These comprehensive characterizations further elucidate the structural attributes of the CuTA nanozyme.

We utilized our previously established method to fabricate fiber-oriented hydrogels through extrusion from a 3D printing nozzle [33]. This method has been demonstrated to successfully prepare oriented cellulose hydrogels. Subsequently, we investigated the rheological properties of the CMHT hydrogel. Fig. S2 b-c illustrates the SEM image and magnified view of the hydrogel after extrusion from the 3D nozzle. The microscopic interior of the hydrogel exhibits a directional arrangement of fibers and honeycomb-like pores, facilitating the transmission of nutrients and creating conditions conducive to the directed proliferation and migration of cells.

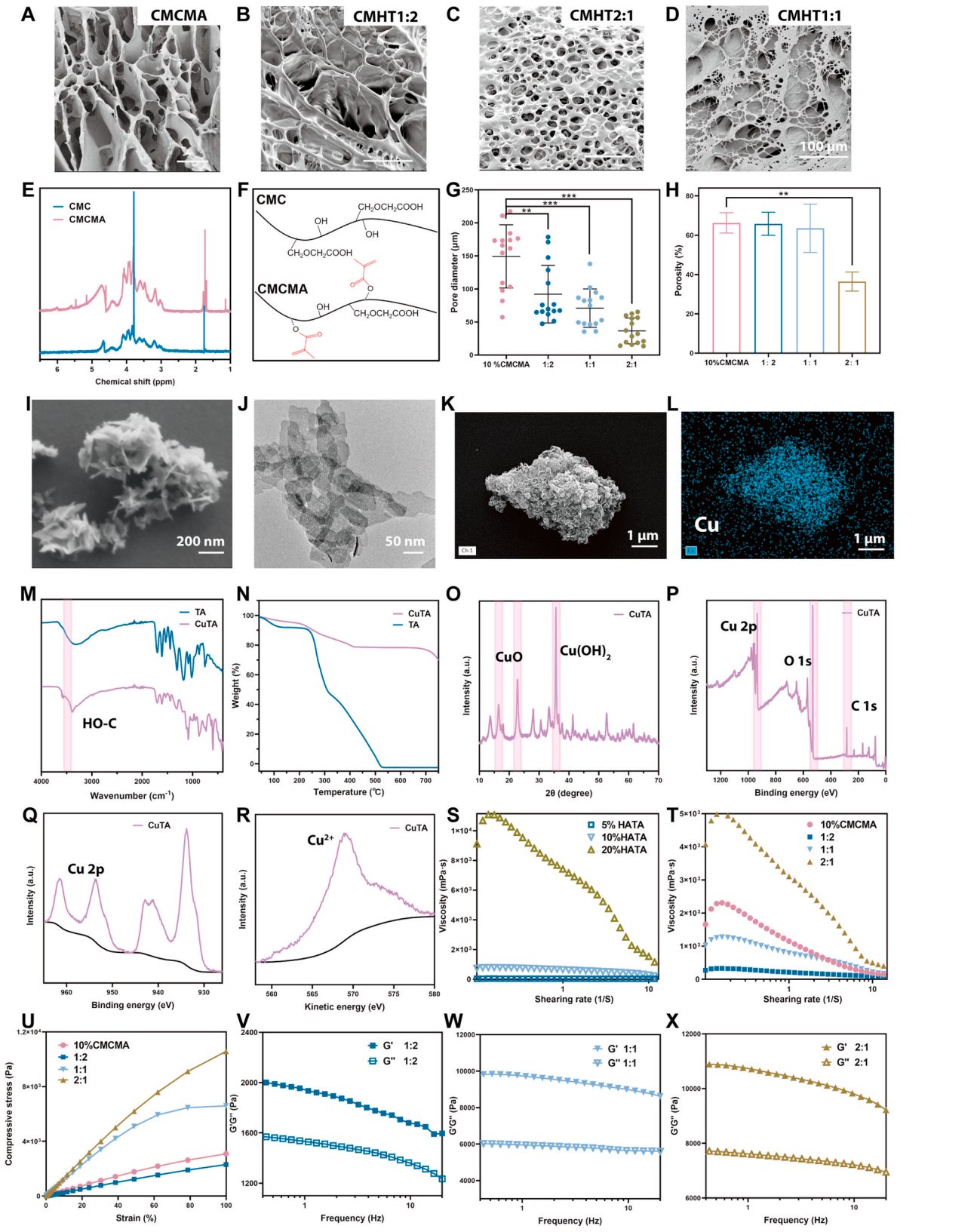

Fig. 1. Preparation and characterization of CuTA-CMHT hydrogel. (A–D) SEM images of cross-section and surfaces of CMHT hydrogel at (CMCMA: HATA at 1:2, 2:1, and 1:1). (E, F) 1H NMR spectrum and structure of CMC, CMCMA. (G, H) Pore size and porosity of CMHT hydrogels (**$P < 0.01$,and ***$P < 0.001$). (I–K) SEM & TEM image of CuTA nanozyme with nanosheet morphology. (L) The element distribution of copper element in the CuTA nanozyme. (M) FTIR spectra of TA and CuTA. (N) Thermogravimetric analysis of TA and CuTA. (O) XRD pattern of CuTA. (P) XPS spectrum and (Q) high-resolution spectrum of Cu 2p of CuTA. (R) Cu LMM Auger spectra of CuTA. (S, T) Continuous flow tests of different HATA, CMCMA hydrogel precursors at shear rates of 0–10 s^{-1}. (U) Compressive stress-strain curves of hydrogels with different proportion of CMHT hydrogel. (V–X) Oscillatory frequency sweep of CMHT hydrogel precursors at different proportion (G': storage modulus, G'': loss modulus).

To investigate the alignment of CuTA-CMHT hydrogels induced by flow, 2D-WAXD measurements were conducted [36]. Calculations based on Equations (S1-5) revealed that the cellulose nanofibers (CNF) within CuTA-CMHT hydrogels exhibited directional alignment after extrusion ($\pi = 80.8$ %, $f = 0.39$) (Fig. S2) compared to their orientation before extrusion ($f = 0.01$, Fig. S2d). These findings confirm the ability of cellulose nanofibers (CNF) in CuTA-CMHT hydrogels to align following extrusion from the nozzle.

Moreover, the CMHT hydrogel precursors exhibit shear-thinning behavior at high shear rates, as indicated by the shearing rate-viscosity curves, suggesting their suitability for printing under equivalent shear rates (Fig. 1 S&T). After the cross-linking and subsequent UV curing of the CMHT hydrogel, it demonstrates elastic properties with G′ greater than G″ (Fig. 1V–X). With an increase in concentration ratios, the content of CMCMA also increases. The compression stresses of CMHT hydrogel with concentration ratios of 2:1 and 1:1 reach 10.5 kPa and 5.5 kPa, respectively, which are 3.5 times and 2 times higher than the compression stress of the single network CMCMA hydrogel (Fig. 1 U). The composite CMHT network hydrogel demonstrates superior mechanical performance.

3.2. Antifungal properties of CuTA-CMHT hydrogel

As fungal keratitis is a condition resulting from fungal infections, *Candida albicans*, *Aspergillus niger*, and *Fusarium solani* were selected as representative fungi associated with fungal keratitis to evaluate the fungistatic efficacy of CMHT-CuTA. Different concentrations of CuTA-CMHT hydrogel were co-cultured with the above fungus for 48 h. Following the plating and incubation of the co-culture solution at 28 °C for 3–7 days, fungal colonies are observed. It is evident that with an increase in CuTA-CMHT concentration, there is a corresponding decrease in the number of colonies (Fig. 2A–C). The fungistatic rate increase with rising concentrations of the CuTA nanozyme. Notably, containing 200 and 100 μg/mL CuTA in CuTA-CMHT hydrogel exhibited superior antifungal effects, surpassing those of fluconazole (Flu) at equivalent concentrations (Fig. 2D–F). Further SEM examination of fungal morphology revealed that with an increase in CuTA concentration, the fungal biofilm became more fragmented and shrunken (Fig. 2G–I), indicating the robust antifungal activity of CuTA-CMHT in effectively disrupting the biofilm and inactivating the fungus. In addition, the efficacy of CuTA in eliminating *Candida albicans* biofilm was additionally confirmed through crystal violet staining. Fig. S3 illustrates that as the concentration of CuTA increases, the CuTA-CMHT hydrogel exhibits an enhanced eradication effect on the biofilm, demonstrating the outstanding biofilm eradication performance of CuTA-CMHT.

3.3. Effectively scavenging ROS properties and In vitro anti-inflammatory effect of CuTA-CMHT hydrogel

The CuTA-CMHT hydrogel exhibits antioxidant properties and effectively alleviates oxidative stress damage by scavenging reactive oxygen species (ROS), including H_2O_2 and $\cdot O^{2-}$. According to existing literature, natural polyphenols like tannic acid (TA) belong to a class of plant secondary metabolites associated with pyrogallol, demonstrating diverse biological activities such as excellent biocompatibility, antioxidant, and anti-inflammatory effects. In the context of our study, CuTA-CMHT hydrogel samples demonstrated a protective role against oxidative stress in corneal epithelial cells under pathological conditions. Corneal epithelial cells were co-cultured with 100 μm H_2O_2 and different concentrations of CuTA-CMHT for 24 h. The intracellular reactive oxygen species (ROS) were evaluated using the fluorescent indicator 2,7 dichlorodihydrofluorescein diacetate (DCFH) and observed under a fluorescence microscope (Fig. 3A–G). Elevated green fluorescence levels indicate higher concentrations of ROS. Fig. 3F and G reveal that the CuTA-CMHT groups at concentrations of 200 and 100 μg/mL displayed significantly lower intracellular ROS levels compared to the H_2O_2 group. This suggests that CuTA-CMHT effectively eliminates ROS, demonstrating its potent antioxidant capabilities (Fig. 3H).

As depicted in Fig. 3I and J, CuTA-CMHT demonstrates the capacity to eliminate $\cdot O^{2-}$ and simulate catalase (CAT) in eliminating H_2O_2. Consequently, when exposed to an oxidative microenvironment, CuTA-CMHT effectively eliminate ROS, achieving antioxidation and alleviating oxidative stress damage. The remaining H_2O_2 production was quantified at 405 nm using the $(NH_4)_2MoO_4$ method, and the simulated catalase (CAT) activity of CuTA-CMHT hydrogel was determined. With an increase in CuTA-CMHT hydrogel concentration, CAT activity escalates, indicating its proficient H_2O_2 removal capability (Fig. 3J). Moreover, the Superoxide Dismutase (SOD) assay kit (WST-1 method) to assess CuTA-CMHT's eliminating ability for $\cdot O^{2-}$. The findings reveal CuTA-CMHT hydrogel's effectiveness in eliminating $\cdot O^{2-}$ (Fig. 3I). The scavenging ability strengthens with higher concentrations, underscoring its robust capability to eliminate ROS.

Immunoregulatory effect of CuTA-CMHT was further investigated via LPS-triggered macrophages model and *Candida albicans*-triggered corneal epithelial cells model. As is known, two phenotypes of macrophages have been recognized as pro-inflammatory (M1) and anti-inflammatroy (M2) ones. In fungal keratitis, macrophages can shift phenotypes and act as important immunomodulatory agents in inflammatory responses [34,37–39]· Triggered by LPS, the macrophages exhibit an elongated shape (M2 cells) compared with M1 cells, and decreased M2 cells were observed after treated with CuTA-CMHT (Fig. S4). This indicating that inflammatory responses could be inhibited by CuTA-CMHT. As shown in Fig. S5, LPS promoted production of IL-1β and IL-6, the representatives of M1-related pro-inflammatory cytokines, which can be inhibited by CuTA-CMHT. To simulate *Candida albicans*-induced inflammatory response, we additionally incubated corneal epithelial cells with inactived *Candida albicans* [35]. After *Candida albicans* stimulation, IL-1β and IL-6 were markedly upregulated, with cell rounding and detachment observed (Fig. S6). CuTA-CMHT intervention inhibited not only the expression of IL-1β and IL-6 but also the *Candida albicans*-induced celluar damage (Fig. S7).

3.4. Contact-guidance effect of cells on patterned groove hydrogels

To assess the ability of oriented-CuTA-CMHT hydrogel scaffolds to induce cell orientation, we employed CuTA-CMHT hydrogel with various ratios to investigate the stability of the printed scaffold. Upon comparison, it was observed that the 3D structure printed using the 1:1 composite hydrogel, among the three ratios, exhibited greater stability and more uniform lines (Fig. S8).

Furthermore, we employed 3D printing in conjunction with a secondary patterned groove design to fabricate oriented-CuTA-CMHT hydrogel, facilitating the alignment of cellulose at both macro and micro levels and significantly enhancing the induction of cell orientation. The cytotoxicity assay results indicated that the cell survival rate for the 100 μg/mL CuTA-CMHT hydrogel was approximately 80 % on day 7 (Fig. S9). Live and dead cell staining further confirmed the predominance of live cells (Fig. S10). To evaluate the impact of the hydrogels on cell migration, a scratch assay was performed (Fig. S11). After 24 h of co-culture with the CuTA-CMHT hydrogel, corneal epithelial cells demonstrated significantly higher migration efficiency compared to both the control group and the CMHT group.

In order to prove the directional arrangement of cells. We seeded the stromal cells on hydrogels scaffold (Fig. S12). In the comparison between Fig. 3K and L, corneal stromal cells exhibited disorderly migration on the no pattern hydrogel structure (Fig. 3K). Conversely, within the secondary patterned groove structure, corneal stromal cells displayed a directional trend in the Ridge and Valley Region (Fig. 3L-N). We quantified the number of cells in different directions, revealing that 90 % of the cells were aligned along the ridges and valleys (Fig. 3O-Q).

Literature reports suggest that cells can recognize surface features of materials, adjusting their size, adhesion, and migration along specific

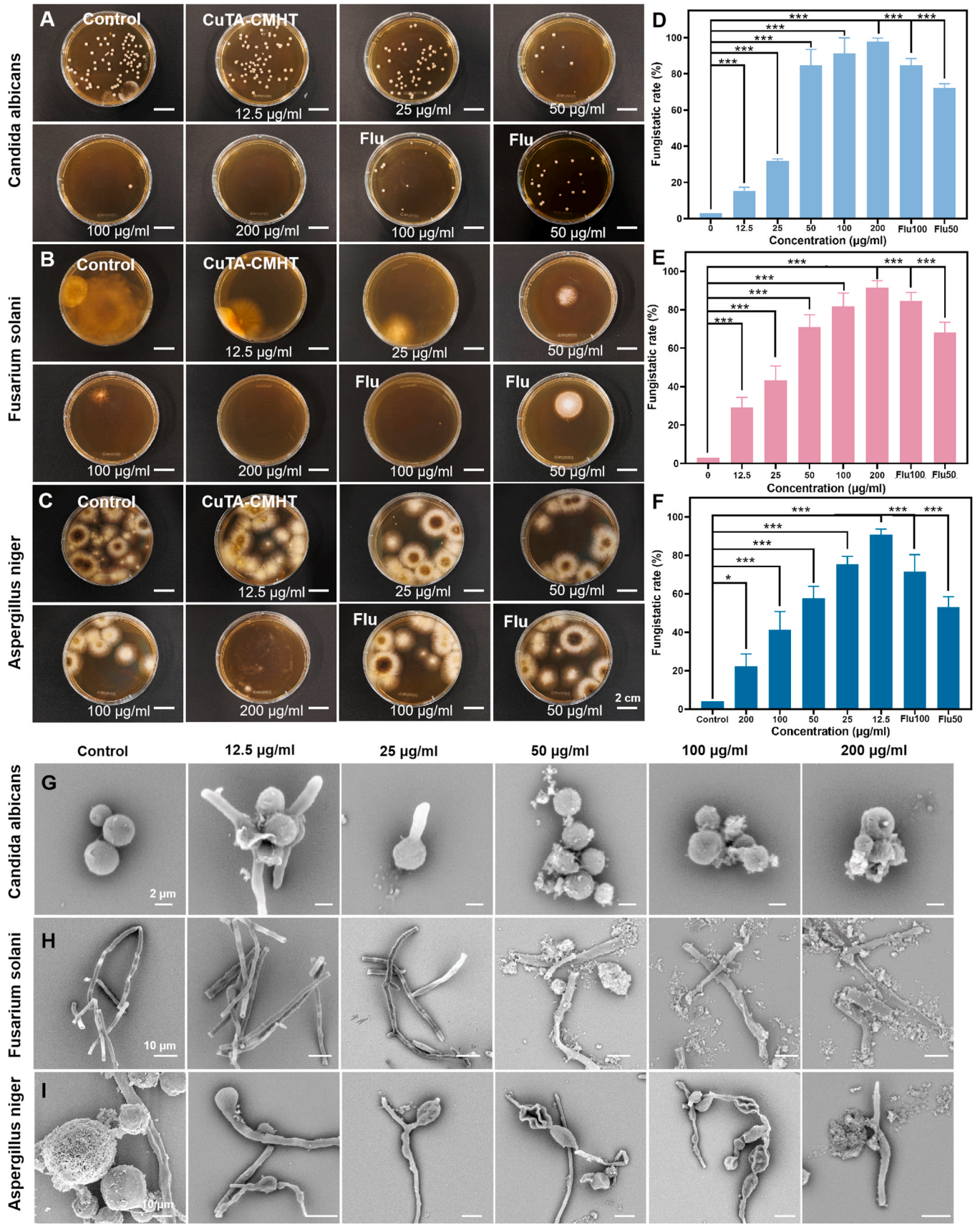

Fig. 2. (A–C) Photographs of fungus colonies formed by *Candida albicans*, *Fusarium solani*, and *Aspergillus niger* after treated by CuTA-CMHT hydrogel samples and Fluconazole (Flu). (D–F) The fungistatic rate of CuTA-CMHT at different concentrations against these three fungi (*$P < 0.05$, **$P < 0.01$,and ***$P < 0.001$). (G–I) SEM images of the above fungus treated with different concentrations of CuTA-CMHT: (1) 0 μg/mL; (2) 12.5 μg/mL; (3) 25 μg/mL; (4) 50 μg/mL; (5) 100 μg/mL; (6) 200 μg/mL.

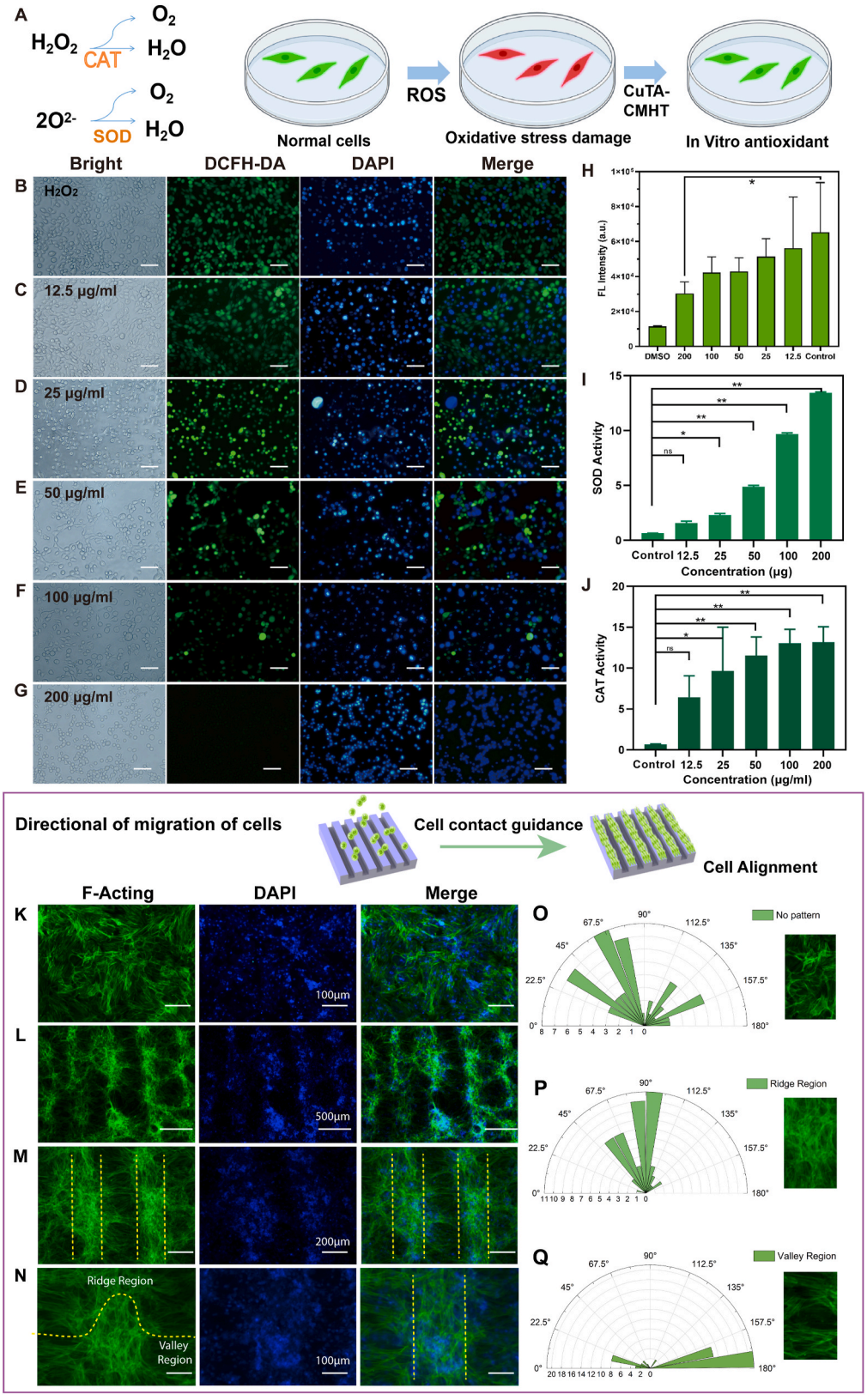

Fig. 3. (A–H) Antioxidant properties of CuTA-CMHT hydrogel. (A) Schematic diagram of alleviating oxidative stress of CuTA-CMHT hydrogel. (A–G) Fluorescence images of corneal epithelial cells upon different concentration of CuTA-CMHT treatments. (H) Quantification of ROS levels in epithelial cells. (I) The SOD mimicry activity of hydrogel samples was studied by WST-1 method. (J) The CAT mimicry activity of hydrogel samples was studied by Ammonium molybdate method (*$P <$ 0.05, **$P < 0.01$). (K–Q) Schematic diagram of Contact-guidance effect of corneal stromal cells on secondary patterned groove hydrogels. (K) Corneal stromal cells were cultured on non-patterned hydrogels. (L) Corneal stromal cells were cultured on 3D printed secondary patterned groove hydrogel scaffolds. (M) Enlarged images of J. (N) Details of cells on the ridge and valley region. (M – O) Quantified the number of cells in different directions.

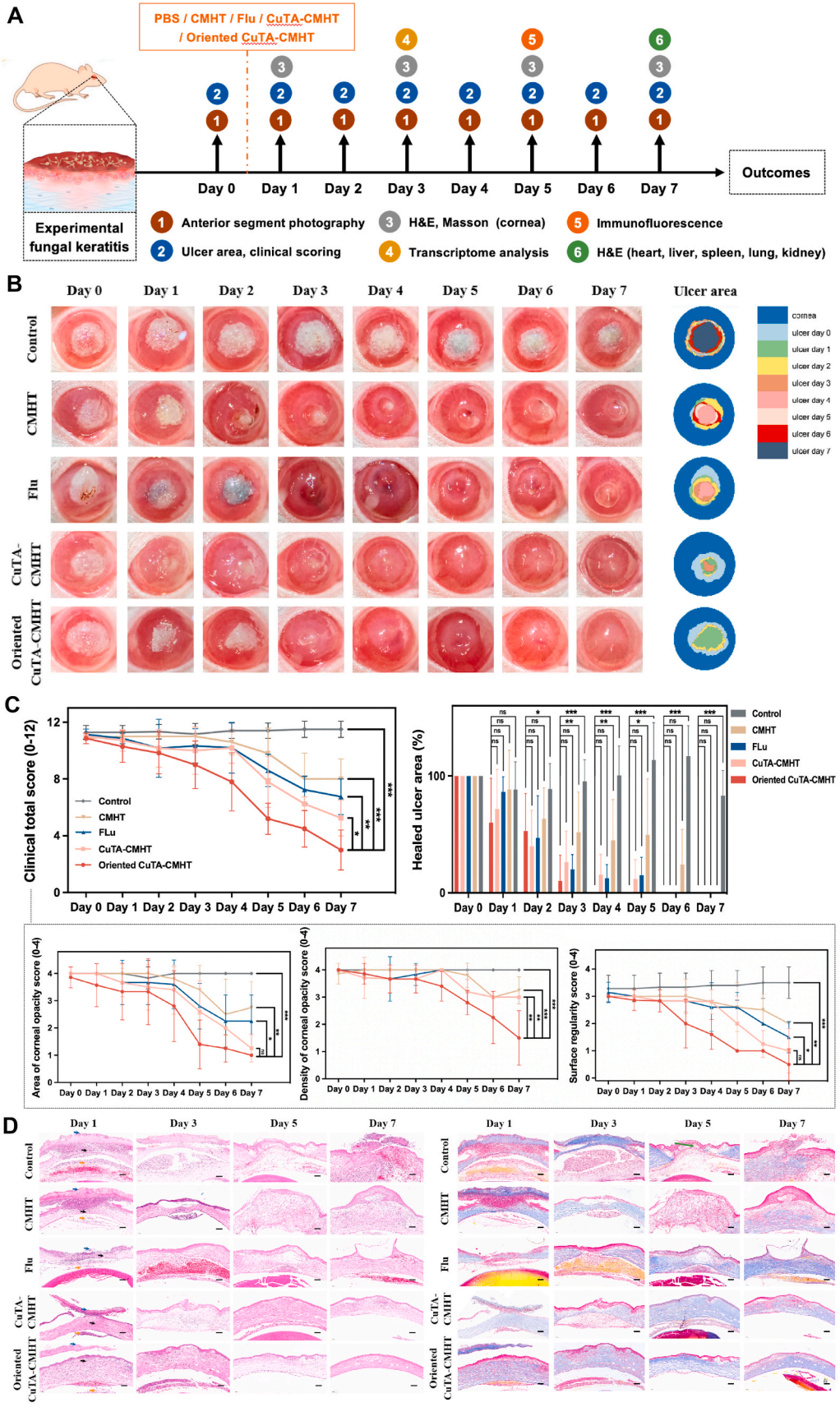

(caption on next page)

Fig. 4. (A) Schematic diagram of the therapeutic efficacy of the oriented CuTA-CMHT was investigated for 7 consecutive days in rat model of fungal corneal ulcer. (B) Ocular surface conditions of rat corneas infected with different treatments over a seven-day period. (C) Quantitative data of healed ulcer area. The disease severity was quantified by clinical total score: area of corneal opacity, density of corneal opacity, and surface regularity. (D) Representative HE staining of the pathological differences in the 5 groups on days 1, 3, 5, and 7. Scale bar, 200 μm. Blue arrow: hyphal development; Black arrow: cornea; Orange arrow: inflammatory infiltration; Green arrow: corneal tissue destruction and dissolution.(*$P < 0.05$, **$P < 0.01$, ***$P < 0.001$).

directions in response to topological structures, resulting in highly oriented cell patterns [40,41]. The grooves on the material's surface can impact the balance of cell arrangement, compelling cells to rearrange themselves to adapt to the contacted hydrogel. These grooves can also regulate signal transduction between cells and the extracellular matrix (ECM), affecting cell adhesion, cytoskeletal development, and cell movement [42].

We hypothesized that cells could interact with the ECM in the corneal stromal layer, influencing signaling pathways. Additionally, we speculated that cells have the potential to form oriented collagen fibers, thereby promoting the directional repair of the corneal stroma.

3.5. Therapeutic efficacy on fungal corneal ulcer in vivo

The therapeutic efficacy of the oriented CuTA-CMHT was investigated for 7 consecutive days in a rat model of fungal corneal ulcer (Fig. 4A) [43,44].After infection with 1×10^6 colony-forming units (CFU)/mL *Candida albicans*, the corneas were manifested as ulcers, stromal edema, stromal opacity, and neovascularization. From day 1–7 after therapy, the 4 treated groups were gradually improved to a varying degree, with healing of ulcer, decreases in opacity area, and regression of neovascularization, especially the oriented CuTA-CMHT group (Fig. 4B). To further evaluate the function of these therapies, the disease severity was quantified by clinical total score with 3 components, including area of corneal opacity, density of corneal opacity, and surface regularity (Table S1) [43]. As shown in Fig. 4C, clinical total scores and the 3 subscale scores were all reduced in the 4 treated groups when compared to the control group. In particular, on day 7, eyes treated with oriented CuTA-CMHT showed significantly lower clinical total scores and density of corneal opacity scores than those treated with CuTA-CMHT, fluconazole, and CMHT. In addition, though there was no significant difference in the other 2 subscale scores and ulcer healing velocity of the oriented CuTA-CMHT group and the CuTA-CMHT group, the indicators were obviously distinct in the oriented CuTA-CMHT group when compared to the fluconazole and the CMHT groups (Fig. 4C).

Representative images of the pathological differences in the 5 groups on days 1, 3, 5, and 7 were shown as Fig. 4D. The control group exhibited hyphal development, corneal tissue destruction and dissolution, fiber fragmentation, inflammatory infiltration, and neovascularization, which were alleviated in the treated groups. As for the oriented CuTA-CMHT group, oriented tissue regeneration was induced with proliferation and directional alignment of collagen fibers as well as removal of hypha and inflammatory cells, corresponding to the almost transparent and smooth reparative tissue in a macroscopic view (Fig. 4A–D). However, corneal tissues were repaired in less ideal manners in the other 3 treated groups. The collagen fibers were relatively irregular in the fluconazole and the CMHT groups, even with bullous formation in the fluconazole group (Fig. 4D). Furthermore, scar tissue was formed in the CMHT group, characterized by haphazardly arranged fibers, thickened epithelium, and numbers of inflammatory and vascular cells (Fig. 4D), which was presented as leukoplakia in Fig. 4A.

As is known, among the azole antifungal agents that widely used in fungal corneal ulcer, fluconazole has been regarded as a more cost-effective and safe antifungals with low toxicity profile [45]. Thus, in this study, fluconazole was performed as a positive control to confirm whether the oriented CuTA-CMHT could represent a promising therapeutic strategy for fungal corneal ulcer management. The comparative results suggested that the oriented CuTA-CMHT did might be an attractive novel therapy because of the dramatic alleviation of keratitis signs, inhibition of inflammation, and regeneration of oriented tissue. Besides, safety of the proposed therapy was also validated, and no obvious inflammation, exudates, necrosis, edema, and other abnormal conditions were observed in heart, liver, spleen, lung, and kidney (Fig. S13).

3.6. Mechanism of induction of oriented tissue regeneration and inhibition of leukoplakia

To figure out the underlying molecular mechanism of oriented CuTA-CMHT-induced oriented tissue regeneration, transcriptome analysis was utilized to identify the mRNA profile changes on day 3. The 3375 differentially expressed genes (DEGs), comprising 2352 upregulated and 1023 downregulated ones, were noted in the fungal corneal ulcer model when compared to the healthy cornea (Fig. 5A and B and Fig. S14). As for the upregulated DEGs, the mainly involved processes are related to inflammation, oxidative stress, and angiogenesis, such as inflammatory response, cellular response to hypoxia, positive regulation of angiogenesis, chemokine activity, cytokine-cytokine receptor interaction, tumor necrosis factor (TNF) signaling pathway, NF-kappa B signaling pathway, hypoxia-inducible factor 1(HIF-1) signaling pathway, etc. (Figs. S15 and S16). While the downregulated DEGs were primarily associated with extracellular matrix (ECM) and cell adhesion, such as ECM organization, ECM structural constituent, integrin binding, collagen-containing ECM, focal adhesion, tight junction, regulation of actin cytoskeleton, phosphatidylinositide 3-kinases (PI3K)- protein Kinase B (AKT) signaling pathway, ECM-receptor interaction, cell adhesion molecules, etc. (Figs. S17 and S18). Among the above leukoplakia-related DEGs, 207 downregulated and 1021 upregulated ones were mitigated after oriented CuTA-CMHT therapy (Fig. 5A and B), which were remarkably more than that after the other 3 therapies. Compared to the control group suffered from fungal corneal ulcer, 1337 DEGs (284 upregulated and 1053 downregulated) were identified in the oriented CuTA-CMHT group (Fig. 5C). Correspondingly, the DEGs were involved in the process and pathways linked to ECM, inflammation, oxidative stress, and angiogenesis, which played important roles in the formation of leukoplakia (Fig. 5D–G). IL-1β and IL-6, as respresentative pro-inflammatory mediators, were also validated to be downregulated in the oriented CuTA-CMHT group (Fig. S19). That is, oriented CuTA-CMHT exhibits a convincing therapeutic effect on ameliorating transcriptome abnormalities in fungal corneal ulcer, through ECM-reorganized, adhesion-regulated, anti-inflammatory, antioxidant, and anti-angiogenesis signaling.

3.7. Efficacy of oriented CuTA-CMHT might be attributed to two aspects: the hydrogel ingredients and the topology

On the one hand, the CuTA nano enzyme functions as an antioxidant, antifungal, anti-inflammatory, and anti-angiogenesis agent, with the CMHT promoting tissue repair. The related alteration of transcriptome map could be observed in the CuTA-CMHT group (Figs. S20 and S21). On the other hand, in respect of topology's role in tissue repairing, 289 DEGs (118 upregulated and 171 downregulated) were recognized in the oriented CuTA-CMHT group when compared to the CuTA-CMHT group (Fig. 6A and Fig. S22). The involved DEGs were mainly related to cell adhesion, such as regulation of actin cytoskeleton, focal adhesion, cell adhesion molecules, actin filament binding, etc. (Fig. 6B and Fig. S23). For actin cytoskeleton and focal adhesion were particularly enriched by both Gene Ontology (GO) and Kyoto Encyclopedia of Genes and

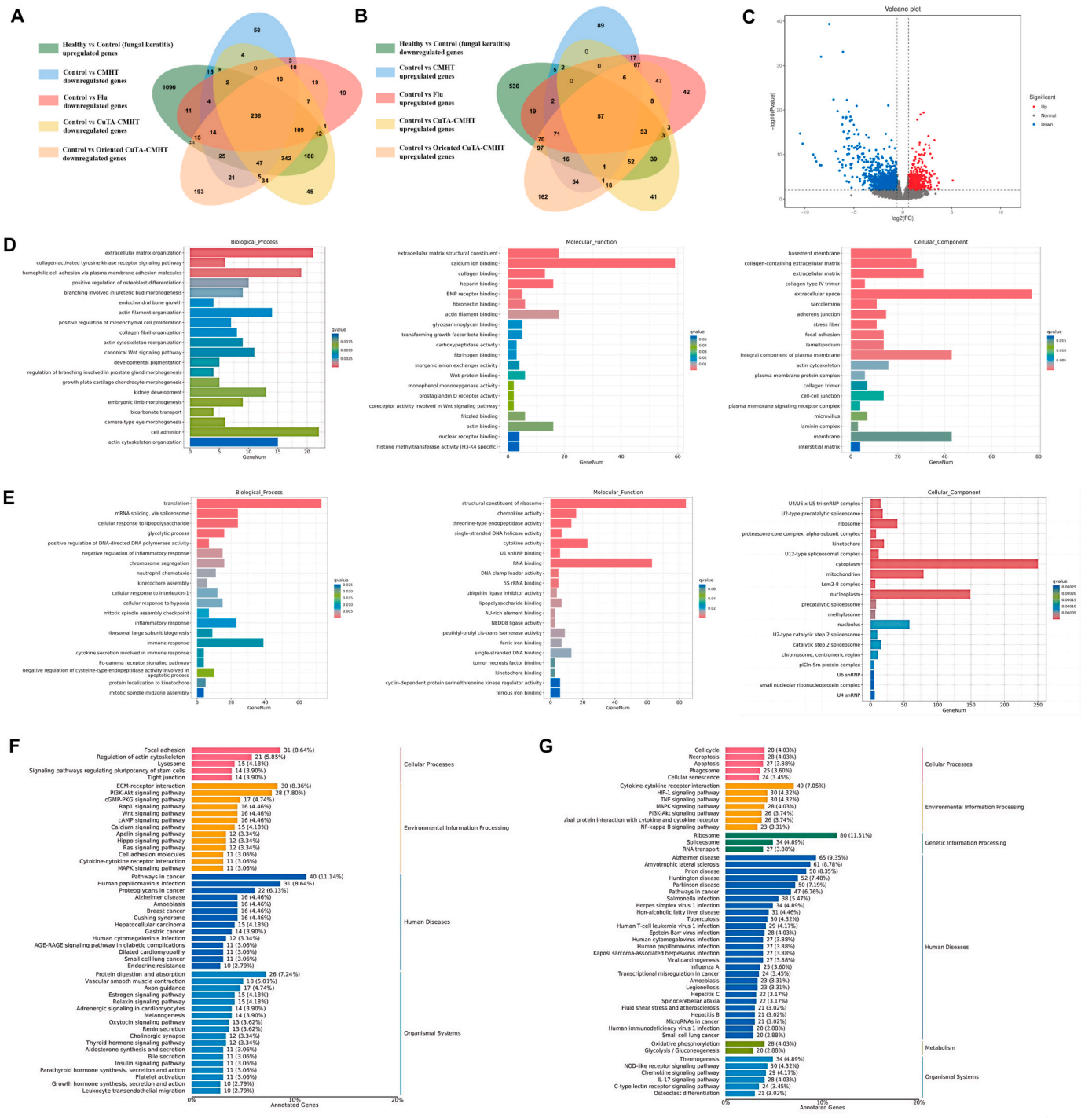

Fig. 5. Transcriptome analysis was utilized to identify the mRNA profile changes on day 3. (A) Venn diagram of downregulated genes in fungal keratitis (compared to healthy cornea) and upregulated genes in the treatment groups (compared to fungal keratitis). (B) Venn diagram of upregulated genes in fungal keratitis (compared to healthy cornea) and downregulated genes in the treatment groups (compared to fungal keratitis). (C) The volcano plot of differentially expressed genes (DEGs) that identified in the oriented CuTA-CMHT group, when compared to the control group with fungal keratitis. (D) The involved biological process, molecular function, and cellular component of upregulated genes in the oriented CuTA-CMHT group. (E) The involved biological process, molecular function, and cellular component of downregulated genes in the oriented CuTA-CMHT group. (F) KEGG pathways associated with upregulated genes in the oriented CuTA-CMHT group. (G) KEGG pathways associated with downregulated genes in the oriented CuTA-CMHT group.

Genomes (KEGG) enrichment analysis, protein–protein interactions (PPIs) of the DEGs involved in these 2 pathways were further explored. Myosin light chain kinase (MYLK) and myosin Light Chain 9 (MYL9) were found to be the core nodes (Fig. 6C and D). Besides, integrins have been regarded as the main cell-adhesion transmembrane receptors that play multifaceted roles as ECM-cytoskeletal linkers and transducers in biochemical and mechanical signals. Among the DEGs that code integrins, integrin subunit alpha 3 (ITGA3) was found to be significantly upregulated in the oriented CuTA-CMHT group than in the CuTA-CMHT group ($P < 0.001$). MYLK, MYL9, and ITGA3 were validated to be mostly expressed in corneas treated with oriented CuTA-CMHT than that with other therapies (Fig. 6E). As is reported, these 3 genes implicated in

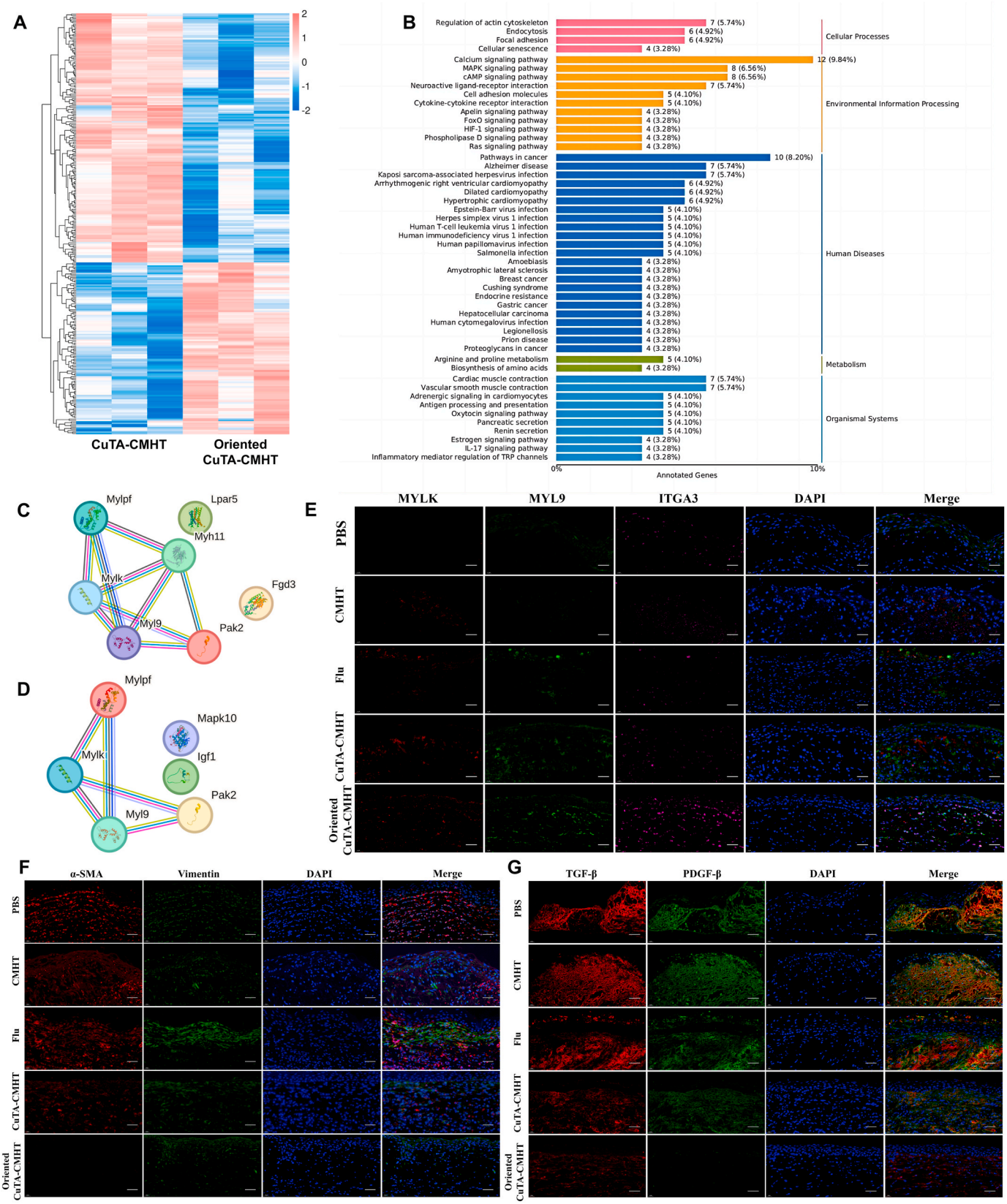

Fig. 6. (A) Differentially expressed genes (DEGs) recognized in the oriented CuTA-CMHT group, compared to the CuTA-CMHT group. (B) KEGG analysis of DEGs in the oriented CuTA-CMHT group (compared to the CuTA-CMHT group). The involved DEGs were mainly related to cell adhesion: regulation of actin cytoskeleton, focal adhesion, cell adhesion molecules, actin filament binding. (C, D) MYLK and MYL9 were the core nodes in protein-protein interaction analysis (PPI) of actin cytoskeleton and focal adhesion. (E) Immunofluorescent assessment of MYLK, MYL9, and ITGA3 expression in corneas subjected to distinct treatments. (F) Immunofluorescence analysis of the amount of α-SMA labeled myofibroblasts in the cornea under different treatments. (G) Immunofluorescent assessment of growth factors TGF-β and PDGF-β expression in corneas. Scale bar = 40 μm.

promoting cell migration and protrusion formation [46–48].

Maintenance of corneal transparency in stromal ulcer healing is centered on ECM and keratocytes [49]. In corneal ulcer, keratocytes were activated to repair the stroma and the stromal repair process can be conducted in 2 different forms: normal-type ECM made by fibroblasts (collagenous) and scar-type ECM made by myofibroblasts (fibrocollagenous) [49]. Myofibroblasts marked by α-smooth muscle actin (α-SMA) were found to be extremely low expressed in corneas treated by oriented CuTA-CMHT (Fig. 6F). Furthermore, weak expression of transforming growth factor beta (TGF-β) and platelet-derived growth factor beta (PDGF-β), which have been identified as components that simulated keratocytes to become myofibroblasts [50,51], were detected in the oriented CuTA-CMHT groups (Fig. 6G).

4. Conclusion

To sum up, the oriented CuTA-CMHT hydrogel fulfils multidimensional roles when treating fungal corneal ulcer (Scheme 1F). Firstly, as the ingredients, CuTA exerts antioxidant, antifungal, anti-inflammatory, and anti-angiogenesis characteristics by inhibiting TNF signaling pathway, NF-kappa B signaling pathway, HIF-1 signaling pathway, and other signals, while CMHT promotes healing through activating signals such as PI3K-AKT signaling pathway. Secondly, due to contact guidance, the oriented topology of the hydrogel induces oriented arrangement of cells in corneal stroma [52]. Protrusion of fibroblasts senses the topology of hydrogel component and orient themselves parallel to the micropatterned lines, promoting elongated cell shape and directional migration. In addition, the fibroblasts also interacted with ECM of corneal stroma through formation of focal adhesions. The processes are associated with molecules such as MYLK, MYL9, and ITGA3. Finally, downregulation of growth factors, such as TGF-β and PDGF-β, inhibits the development of myofibroblasts and reduces the production of scar-type ECM. Therefore, the oriented CuTA-CMHT hydrogel struggles with fungal corneal ulcer and induces oriented tissue regeneration upon biochemical and mechanical mechanisms. It exhibits considerable potential for treating fungal corneal ulcers and leukoplakia, representing a potential milestone in the field of corneal tissue engineering.

Ethics approval and consent to participate

All the protocols for animal experiments were approved by the Institutional Animal Care and Use Committee of Tsinghua University and conducted in accordance with the Association for Research in Vision and Ophthalmology statement for the use of animals in ophthalmic vision and research.

CRediT authorship contribution statement

Lina Dong: Writing – original draft, Validation, Investigation, Data curation. **Zixin Fan:** Writing – original draft, Investigation. **Bixing Fang:** Validation, Methodology. **Xiaoyu Zhao:** Visualization, Software. **Hongyi Yao:** Software. **Gangpei Cai:** Formal analysis, Data curation. **Shuo Yang:** Methodology. **Guoming Zhang:** Supervision. **Xiaoqi Cheng:** Visualization. **Yun Feng:** Supervision, Funding acquisition. **Shengli Mi:** Supervision, Funding acquisition. **Wei Sun:** Writing – review & editing, Supervision, Funding acquisition.

Declaration of competing interest

The authors declare that they have no known competing financial interests or personal relationships that could have appeared to influence the work reported in this paper.

Acknowledgments

The authors acknowledge financial support from the Tsinghua Berkeley Shenzhen Institute and the Project of Basic Research of Shenzhen, China (JCYJ20170412101508433 & JCYJ20180507183655307); The National Key Research and Development Program of China (2023YFE0203100) and the National Natural Science Foundation of China (Grant Nos. 82271051, 82070926).

Appendix A. Supplementary data

Supplementary data to this article can be found online at https://doi.org/10.1016/j.bioactmat.2024.07.008.

References

[1] C. Brunner-Mendoza, C. Guerrero-Guerra, O. Villagomez-Figueroa, H. Navarro-Barranco, A. Perez-Mejia, C. Toriello, A review of described cases of mycotic keratitis and sclerokeratitis related to entomopathogenic fungi from 1984 to 2021, J. Mycolog. Med. 32 (2) (2022).
[2] S. Mahmoudi, A. Masoomi, K. Ahmadikia, S.A. Tabatabaei, M. Soleimani, S. Rezaie, H. Ghahvechian, A. Banafsheafshan, Fungal keratitis: an overview of clinical and laboratory aspects, Mycoses 61 (12) (2018) 916–930.
[3] A.C. Alvarez-de-Carvalho, H. Iran-Ruthes, M. Maia, D. Yana, M. Teruo-Sato, H. Moreira, G. Fernandes-Bordignon, F. de-Queiroz-Telles, Fungal keratitis in the State of Parana-Brazil: clinical, epidemiological and diagnostic findings, Rev. Iberoam. De. Micol. 18 (2) (2001) 76–78.
[4] L. Brown, A.K. Leck, M. Gichangi, M.J. Burton, D.W. Denning, The global incidence and diagnosis of fungal keratitis, Lancet Infect. Dis. 21 (3) (2021) 49–57.
[5] S.P. Sharma, S. Dwivedi, S. Kumar, K. Dhama, A.K. Sharma, Bacterial and fungal keratitis: current trends in its diagnosis and management, Curr. Clin. Microbiol. Rep.10 (2023) 266–278.
[6] L. Gu, J. Lin, Q. Wang, L. Zhang, M. Yin, H. Lin, H. Zheng, G. Zhao, C. Li, Dimethyl fumarate ameliorates fungal keratitis by limiting fungal growth and inhibiting pyroptosis, Int. Immunopharm. 115 (2023).
[7] P. Niu, Y. Wu, F. Zeng, S. Zhang, S. Liu, H. Gao, Development of nanodrug-based eye drops with good penetration properties and ROS responsiveness for controllable release to treat fungal keratitis, NPG Asia Mater. 15 (1) (2023).
[8] S.M. Leal, Fungal Keratitis: Immune Recognition, Neutrophil-Hyphae Interactions, and Fungal Anti-oxidative Defenses, 2012.
[9] K. Ichikawa, T. Ono, L. Chen, K. Kitamoto, Y. Taketatni, T. Toyono, J. Yoshida, M. Aihara, T. Miyai, Quantitative Evaluation of Corneal Irregularity and Scarring after Infectious Keratitis Using Anterior Segment Optical Coherence Tomography, Graefes Archive for Clinical and Experimental Ophthalmology, 2023.
[10] S.A. Menda, M. Das, A. Panigrahi, N.V. Prajna, N.R. Acharya, T.M. Lietman, S. D. McLeod, J.D. Keenan, Association of post-fungal keratitis corneal scar features with visual acuity, Jama Ophthalmology 138 (2) (2020) 113–118.
[11] Y. Zhou, Y. Chen, S. Wang, F. Qin, L. Wang, MSCs helped reduce scarring in the cornea after fungal infection when combined with anti-fungal treatment, BMC Ophthalmol. 19 (1) (2019).
[12] Z. Ansari, D. Miller, A. Galor, Current thoughts in fungal keratitis: diagnosis and treatment, Current Fungal Infection Reports 7 (3) (2013) 209–218.
[13] L. Gu, C. Li, J. Lin, Q. Wang, M. Yin, L. Zhang, N. Li, H. Lin, Z. You, S. Wang, D. Li, G. Zhao, Drug-loaded mesoporous carbon with sustained drug release capacity and enhanced antifungal activity to treat fungal keratitis, Biomater. Adv. 136 (2022).
[14] J.-F. Huang, J. Zhong, G.-P. Chen, Z.-T. Lin, Y. Deng, Y.-L. Liu, P.-Y. Cao, B. Wang, Y. Wei, T. Wu, J. Yuan, G.-B. Jiang, A hydrogel-based hybrid theranostic contact lens for fungal keratitis, ACS Nano 10 (7) (2016) 6464–6473.
[15] J. Wu, W.-S. Zhang, J. Zhao, H.-Y. Zhou, Review of clinical and basic approaches of fungal keratitis, Int. J. Ophthalmol. 9 (11) (2016) 1676–1683.
[16] W.M. Nada, M.A. Al Aswad, W.M. El-Haig, Combined intrastromal injection of amphotericin B and topical fluconazole in the treatment of resistant cases of keratomycosis: a retrospective study, Clin. Ophthalmol. 11 (2017) 871–874.
[17] L. Chen, D. Yan, N. Wu, Q. Yao, H. Sun, Y. Pang, Y. Fu, Injectable bio-responsive hydrogel for therapy of inflammation related eyelid diseases, Bioact. Mater. 6 (10) (2021) 3062–3073.
[18] X. Cheng, H. Chen, F. Yang, J. Hong, Y. Cheng, J. Hu, All-small-molecule supramolecular hydrogels assembled from guanosine 5′-monophosphate disodium salt and tobramycin for the treatment of bacterial keratitis, Bioact. Mater. 16 (2022) 293–300.
[19] H. Zhou, S. Zhang, M. Lei, Y. Cai, H. Wang, J. Sun, J. Cui, C. Liu, X. Qu, A suture-free, shape self-adaptive and bioactive PEG-Lysozyme implant for corneal stroma defect repair and rapid vision restoration, Bioact. Mater. 29 (2023) 1–15.
[20] J. He, Y. Ye, D. Zhang, K. Yao, M. Zhou, Visualized gallium/lyticase-integrated antifungal strategy for fungal keratitis treatment, Adv. Mater. 34 (49) (2022).
[21] B. Kong, R. Liu, X.J. Hu, M.Y. Li, X.T. Zhou, Y.J. Zhao, T.T. Kong, Cornea-inspired ultrasound-responsive adhesive hydrogel patches for keratitis treatment, Adv. Funct. Mater. 34 (2023) 2310544–2310554.
[22] S. Liu, Q. Bai, Y. Jiang, Y. Gao, Z. Chen, L. Shang, S. Zhang, L. Yu, D. Yang, N. Sui, Z. Zhu, Multienzyme-like nanozyme encapsulated ocular microneedles for keratitis treatment, Small 20 (2023) 2308403–2308419.
[23] Y. Ye, J. Yu, C. Wang, N.-Y. Nguyen, G.M. Walker, J.B. Buse, Z. Gu, Microneedles integrated with pancreatic cells and synthetic glucose-signal amplifiers for smart insulin delivery, Adv. Mater. 28 (16) (2016) 3115–3121.

[24] B. Kong, R. Liu, J. Shan, M. Li, X. Zhou, Y. Zhao, Frozen reinforced microneedles loaded with NIR-photothermal nanozyme for keratitis treatment, Nano Today 52 (2023).
[25] M.A. Saccone, R.A. Gallivan, K. Narita, D.W. Yee, J.R. Greer, Additive manufacturing of micro-architected metals via hydrogel infusion, Nature 612 (7941) (2022) 685.
[26] B.E. Kelly, I. Bhattacharya, H. Heidari, M. Shusteff, C.M. Spadaccini, H.K. Taylor, Volumetric additive manufacturing via tomographic reconstruction, Science 363 (6431) (2019) 1075.
[27] E. Ilhan, S. Cesur, R.B. Sulutas, E. Pilavci, B. Dalbayrak, E. Kaya, E.D. Arisan, G. B. Tinaz, M. Sengor, E. Kijeenska-Gawaronska, F.N. Oktar, O. Gunduz, The role of multilayer electrospun poly(vinyl alcohol)/gelatin nanofibers loaded with fluconazole and cinnamaldehyde in the potential treatment of fungal keratitis, Eur. Polym. J. 176 (2022).
[28] H.K. Polat, S.B. Pehlivan, C. Ozkul, S. Calamak, N. Ozturk, E. Aytekin, A. Firat, K. Ulubayram, S. Kocabeyoglu, M. Irkec, S. Calis, Development of besifloxacin HCl loaded nanofibrous ocular inserts for the treatment of bacterial keratitis: *In vitro, ex vivo* and *in vivo* evaluation, Int. J. Pharm. 585 (2020).
[29] Z.Z. Zhou, Y. Pang, J.Y. Ji, J.Y. He, T.K. Liu, L.L. Ouyang, W. Zhang, X.L. Zhang, Z. G. Zhang, K.T. Zhang, W. Sun, Harnessing 3D in vitro systems to model immune responses to solid tumours: a step towards improving and creating personalized immunotherapies, Nat. Rev. Immunol. 24 (2023) 18–32.
[30] B. Kong, Y. Chen, R. Liu, X. Liu, C.Y. Liu, Z.W. Shao, L.M. Xiong, X.N. Liu, W. Sun, S.L. Mi, Fiber reinforced GelMA hydrogel to induce the regeneration of corneal stroma, Nat. Commun. 11 (1) (2020) 1435–1447.
[31] Z. Guo, Y. Xu, L. Dong, M.S. Desai, J. Xia, M. Liang, S.-W. Lee, S. Mi, W. Sun, Design of functional hydrogels using smart polymer based on elastin-like polypeptides, Chem. Eng. J. 435 (2022).
[32] Y. Chen, L. Dong, B. Kong, Y. Huang, S. Zhong, C. Connon, J. Tan, S. Yang, W. Sun, S. Mi, Effects of gelatin methacrylate hydrogel on corneal repair and regeneration in rats, Translational Vision Science & Technology 10 (14) (2021).
[33] L. Dong, M. Liang, Z. Guo, A. Wang, G. Cai, T. Yuan, S. Mi, W. Sun, A study on dual-response composite hydrogels based on oriented nanocellulose, International Journal of Bioprinting 8 (3) (2022) 126–139.
[34] B. Tao, W. Yi, X. Qin, J. Wu, K. Li, A. Guo, J. Hao, L. Chen, Improvement of antibacterial, anti-inflammatory, and osteogenic properties of OGP loaded Co-MOF coating on titanium implants for advanced osseointegration, J. Mater. Sci. Technol. 146 (2023) 131–144.
[35] Y. Zhu, X. Peng, Y. Zhang, J. Lin, G. Zhao, Baicalein protects against *Aspergillus fumigatus* keratitis by reducing fungal load and inhibiting TSLP-induced inflammatory response, Invest. Ophthalmol. Vis. Sci. 62 (6) (2021).
[36] X. Le, W. Lu, J. Zhang, T. Chen, Recent progress in biomimetic anisotropic hydrogel actuators, Adv. Sci. 6 (5) (2019).
[37] J. Hu, Y. Wang, L. Xie, Potential role of macrophages in experimental keratomycosis, Invest. Ophthalmol. Vis. Sci. 50 (5) (2009) 2087–2094.
[38] Targeting macrophages in cancer immunotherapy, Signal Transduct. Targeted Ther. 6 (4) (2021) 1212–1232.
[39] Y. Xu, Y. Luo, Z. Weng, H. Xu, W. Zhang, Q. Li, H. Liu, L. Liu, Y. Wang, X. Liu, L. Liao, X. Wang, Microenvironment-responsive metal-phenolic nanozyme release platform with antibacterial, ROS Scavenging, and Osteogenesis for Periodontitis, ACS Nano 17 (19) (2023) 18732–18746.
[40] J. Kim, W.-G. Bae, Y.J. Kim, H. Seonwoo, H.-W. Choung, K.-J. Jang, S. Park, B. H. Kim, H.-N. Kim, K.S. Choi, M.-S. Kim, P.-H. Choung, Y.-H. Choung, J.H. Chung, Directional matrix nanotopography with varied sizes for engineering wound healing, Adv. Healthcare Mater. 6 (19) (2017).
[41] F. Zhou, L. Yuan, Y. Mei, H. Chen, Effects of contact guidance and gravity on L929 cell orientation, Chin. Sci. Bull. 56 (10) (2011) 977–981.
[42] M.J. Dalby, R.O.C. Oreffo, Skeletal Stem Cells and Controlled Nanotopography, 2011.
[43] T.G. Wu, K.R. Wilhelmus, B.M. Mitchell, Experimental keratomycosis in a mouse model, Invest. Ophthalmol. Vis. Sci. 44 (1) (2003) 210–216.
[44] S.M. Ahsan, C.M. Rao, Condition responsive nanoparticles for managing infection and inflammation in keratitis, Nanoscale 9 (28) (2017) 9946–9959.
[45] P. Lakhani, A. Patil, S. Majumdar, Challenges in the polyene- and azole-based pharmacotherapy of ocular fungal infections, J. Ocul. Pharmacol. Therapeut. 35 (1) (2019) 6–22.
[46] Y. Wang, D. Yang, R. Zhu, F. Dai, M. Yuan, L. Zhang, Y. Zheng, S. Liu, X. Yang, Y. Cheng, YY1/ITGA3 pathway may affect trophoblastic cells migration and invasion ability, J. Reprod. Immunol. 153 (2022) 103666.
[47] Y.-C. Hsu, H.-Y. Chen, S. Yuan, S.-L. Yu, C.-H. Lin, G. Wu, P.-C. Yang, K.-C. Li, Genome-wide analysis of three-way interplay among gene expression, cancer cell invasion and anti-cancer compound sensitivity, BMC Med. 11 (2013).
[48] E. Infante, A. Stannard, S.J. Board, P. Rico-Lastres, E. Rostkova, A.E.M. Beedle, A. Lezamiz, Y.J. Wang, S.G. Breen, F. Panagaki, V.S. Rajan, C. Shanahan, P. Roca-Cusachs, S. Garcia-Manyes, The mechanical stability of proteins regulates their translocation rate into the cell nucleus, Nat. Phys. 15 (9) (2019) 973.
[49] J.R. Hassell, D.E. Birk, The molecular basis of corneal transparency, Exp. Eye Res. 91 (3) (2010) 326–335.
[50] S.E. Wilson, Corneal wound healing, Exp. Eye Res. 197 (2020) 108089.
[51] S.E. Wilson, Defective perlecan-associated basement membrane regeneration and altered modulation of transforming growth factor beta in corneal fibrosis, Cell. Mol. Life Sci. 79 (3) (2022) 144.
[52] S. SenGupta, C.A. Parent, J.E. Bear, The principles of directed cell migration, Nat. Rev. Mol. Cell Biol. 22 (8) (2021) 529–547.